Article

Development of an artificial olfactory system for lubricant degradation monitoring

Bernabei, Mara, Pantalei, Simone and Sherrington, Ian

Bernabei, Mara orcid iconORCID: 0000-0003-4331-6745, Pantalei, Simone and Sherrington, Ian orcid iconORCID: 0000-0003-1283-9850 (2020) Development of an artificial olfactory system for lubricant degradation monitoring. International Journal of Condition Monitoring and Diagnostic Engineering Management, 23 (1). pp. 3-12. ISSN 1363–7681

COMADEM
International Journal of Condition Monitoring and Diagnostic Engineering Management

Development of an artificial olfactory system for lubricant degradation monitoring

Mara Bernabei[a] *, Simone Pantalei[b], and Ian Sherrington[a]

[a]*Jost Institute for Tribotechnology, School of Engineering, University of Central Lancashire, Preston PR1 2HE, UK*
[b]*Ascend Diagnostics Limited, Citylabs 1.0, Nelson St, Manchester, M13 9NQ, Uk*
∗ *Mara Bernabei. Tel.: +44-01772-893260; email: mbernabei@uclan.ac.uk*

ABSTRACT

Off-line strategies are commonly used to evaluate lubricant aging. These methods are expensive, time consuming and often require skilled personnel. On-line detection of lubricant degradation would eliminate some of these issues. Lubricant degradation is principally due to oxidation, additive depletion and contamination by water, acid, fuel, sulphur, and insoluble content which happens gradually through different phases of the lubricant lifetime. The by-products and final products of this chemical process characterise the different evolutive phases of oil aging and are reflected in the volatile compounds emitted by the lubricant while degrading. Hence, the lubricant headspace contains a significant amount of information about oil degradation. This paper reports the development of an artificial olfactory system for real-time oil condition evaluation by headspace analysis. The instrument has been optimised to exhibit high discriminatory power and high sensitivity towards the vapours characterising the oil aging process, while the device costs have been kept low. Preliminary measurements have been carried out on water samples, new engine oil and aged engine oil to evaluate the ability of the system to generate sensor patterns distinctive of the samples under test and to discriminate between new engine oil and relatively aged engine oil. The results of these measurements are presented and discussed in the paper.

Keywords: Artificial Olfactory System; Electronic Nose, Chemical Gas Sensors; Lubricant Degradation; Oil Condition Monitoring

1. Introduction

Longevity and the performance of industrial machinery and combustion engines are preserved by using lubricating oils, which reduce friction and wear between moving parts, remove heat and wear debris, protect from contaminants and slow down the corrosion process [1].

During machine operation, lubricating oil goes through a destructive degradation process that changes its physical, electrical, and chemical properties and reduces its lubricating capability [2]. The degraded performance of the lubricant can cause excessive fatigue and corrosion between parts and can lead to equipment damage and, in the worst case, machine failure. It is fundamental to monitor the oil condition to gain a prompt warning for oil replacement and avoid machine damage and disruption, and unnecessary oil replenishment, which can have significant effects on company finances and the operational environment.

Nowadays, oil condition monitoring happens principally by off-line analysis carried out on regularly collected oil samples. These analyses are time consuming, expensive and often require experienced personnel [3]. Moreover, the collection of the samples can sometimes require machine shut-down. Alternatively, the oil is changed periodically, and often prematurely, without carrying out any testing. These maintenance strategies reduce the risk of machine damage but have an economic impact on company profits. Consequently, on-line health monitoring of lubricants is a demanded approach for industry [4].

Lubricant aging affects the chemical composition of the lubricant oil and of the volatile compounds emitted by the oil. As a consequence, real time oil condition monitoring can be carried out by evaluating the content of the volatile compounds in the headspace above the lubricants [5].

Artificial olfactory systems are devices that emulate biological olfaction and encode the volatile profile of a complex gaseous sample in a pattern of electronic signals. The pattern is a fingerprint of the mixture analysed and it can be processed by means of multivariate data analysis techniques to obtain odour recognition and classification [6, 7].

This paper details the design of an instrument of this type, capable of carrying out simple and rapid odour analysis for on-line oil condition monitoring by detecting variations in the composition of the vapour phase of the lubricant. The strategies adopted to improve its sensitivity and the discriminatory power are highlighted. Preliminary tests have been carried out to evaluate the capability of the instrument to provide repeatable and accurate measurements to discriminate between new and aged engine oil. The results of these measurements are reported and discussed below.

2. Theoretical Background

Conventionally, several oil parameters have been correlated to assess the level of oil degradation these include: viscosity, total base number (TBN), total acid number (TAN), water content, permittivity, conductivity, size and concentration of wear debris, etc.

These properties have been commonly used for reliable and accurate off-line oil analysis [4, 8].

In the last 2 decades, numerous sensor technologies have been developed to measure the variation of these parameters with the final aim of real-time evaluation of lubricant state. However, this goal has not yet been fully achieved. Each on-line strategy considered, presents several advantages, but also exhibits drawbacks that have impeded the development of a reliable, accurate, easy to use and robust monitoring system capable of overcoming the off-line monitoring strategies. The main reason for this failure has been mainly ascribed to the large variety of oil formulations and to the complexity of the degradation process [9].

Viscosity sensors have been extensively studied and developed, and they are highly promising sensors for oil monitoring. However, they suffer various problems including limited reliability due to the influence of wear debris on the speed of the moving body [10]. Acoustic wave viscometers that use quartz crystal microbalances (QCM) are unique for their simplicity, but their output can depend on contaminants in the oil [11]. They also show decreasing accuracy and lifetime while operating, because of the corrosion of sensor parts immersed in the sample [4]. Other acoustic sensors exhibit high sensitivity not only to the viscosity of the medium, but also to oil contaminants and air bubbles [8, 10].

Wear debris sensors based on different technologies have been developed. Commercial wear debris sensors are available, but they have disadvantages, including: limited throughput; low sensitivity to small debris, and influence of water [12,13]. Hence, their application as health oil monitoring is limited.

Lubricant degradation is principally due to oxidation, contamination by water, soot, fuels, acid and insoluble content, and additive depletion [3].

The by-products and final products of the chemical process of oil degradation are well known, and the degradation pathway can be very well defined for many mineral oil formulations: alkyl radicals and hydroperoxides abound in the early stages of the process; aldehydes, alcohols ketones, and carboxylic, sulphur and nitric acids increase in concentration with oil aging [3, 14]. These chemical changes, happening during the aging of the oil, are reflected in the variation of the volatile compounds evaporated from the lubricant oils over time. By monitoring the headspace in lubricant sumps, the variation of the volatile components emitted by the lubricant oil can be detected and oil aging can be evaluated.

Artificial olfactory systems, or electronic noses (e-noses), are instruments that are sensitive to a large number of volatile compounds and they can identify, discriminate and classify different complex vapour samples [15].

They are composed of three main elements [16]:

- A sampling and delivery system, which collect the vapour sample and deliver it to the sensors;
- An array of chemical sensors, which is enclosed in a measurement chamber;
- A pattern recognition engine that performs multivariate analysis on the sensor data.

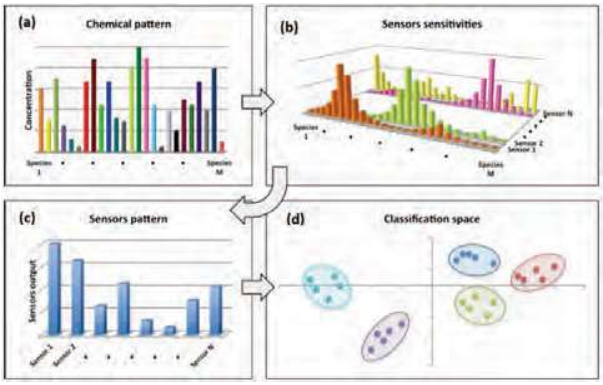

Figure 1. Working principle of an e-nose instrument.

The general working principle of an electronic nose is illustrated in Figure 1. When a complex mixture (Figure 1(a)) is analysed by an e-nose, the sampling system delivers it to the sensor array, avoiding loss or contamination of the sample. The sensor array is made of different, broadly selective sensors. Hence, each sensor detects different volatile compounds with a sensitivity that is characteristic of the sensor and differs from the sensitivity exhibited by the other elements of the array (Figure 1(b)). Thanks to this feature, when the vapour mixture is detected by the array, each sensor generates a signal that is correlated to the whole composition of the mixture. The response of the artificial olfactory system is a pattern of electronic signals that is a fingerprint of the aroma sample (Figure 1(c)) [17]. This pattern contains the chemical information of the entire vapour mixture and is processed with statistical tools by the pattern recognition engine to have odour discrimination and/or classification (Figure 1(d)).

This odour recognition process emulates the principle of biological olfaction, where a wide number of different and broadly specific receptor neurons detect the inhaled odorant molecules and generates a signal that is transmitted to the olfactory bulb and then to the brain where odour recognition happens.

Artificial olfactory systems have been extensively used in analytical laboratories and industries for numerous applications in several different fields: environmental control [18-21], security [22, 23], agricultural and forestry [24, 25], pharmaceutical [26], aerospace [27,28] and more.

In food industries, e-noses have been used to perform quality assessment, shelf life monitoring and food freshness control [29 - 32]. A Fox 4000 electronic nose, commercialised by AlphaMOS, was used to evaluate the shelf life of milk by monitoring the growth of total bacteria [33]. In the pharmaceutical field, the same detector was used to evaluate different qualities and intensities of various flavors used in pharmaceutical formulations [34].

Despite the complexity of human body fluids, a variety of artificial olfactory systems have been tested to diagnose a large number of diseases by detecting the volatile compounds in body fluids as urine, breath, sputum, and sweat [35 - 37]. Cyranose 320 is a commercial electronic nose from Senigent Intelligent Sensing Solutions that has demonstrated the capability of identifying several human illnesses [38 - 40].

Because of the ability of artificial olfaction to characterise complex gaseous samples, they have the potential to detect variations in volatile compounds of the lubricant headspace caused by oil degradation.

The advantages of e-nose compared to traditional analytical instruments include low cost, easy use, short analysis time and small dimensions.

When developing an artificial olfactory instrument for a specific odour analysis, each element of the system needs to be designed and optimised for the scope of the application.

The aim of this project was to develop an analytical instrument of low-cost, which was easy to use and producing real-time oil condition monitoring.

All the components of the instrument were carefully designed to maximise its sensitivity and selectivity to the volatile compounds that are characteristic of the mineral oil degradation processes while minimising cross-sensitivity to interferents and able to produce stable reproducible measurements.

The device development and optimisation is described in section 3.

3. Methodology

The system consists of three broad elements: a chemical sensor array, a read-out circuit and a measurement chamber. Some elements used in the system are commercially available. Other components are bespoke having been carefully designed to improve the capability of the instrument to discriminate between similar oil aging phases.

3.1. *Chemical sensor array*

Many kinds of chemical sensors technologies are available for artificial olfactory devices. They differ in their sensitivity to the volatile compounds, the type of output signal they produce, their robustness to the environmental parameters, power consumption, dimensions and other factors.

For this system, seven commercial metal oxide semiconductor (MOS) sensors were selected. They are part of the TGS family from Figaro Engineering Inc. and are characterised by high sensitivity towards the volatile compounds that are of interest in this application. They are small in size and have relatively low cost. Furthermore, they are robust, being optimised for use in harsh environments and are considered well suited for this project.

The structure of the TGS Figaro sensors is shown in Figure 2

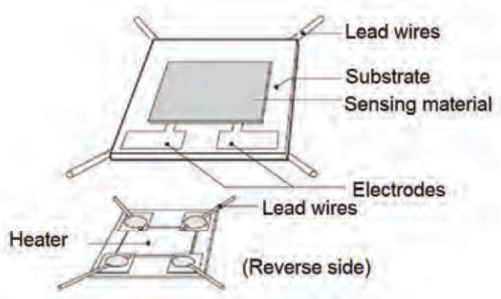

Figure 2. Structure of a TGS sensor produced by the Figaro Engineering Inc.

The sensing element of a MOS sensor is composed of a metal oxide semiconductor film (sensing material in Figure 2) wich is mounted on top of a heater element. In the case of the TGS family, the metal oxide semiconductor is tin-oxide.

When the metal oxide layer is heated to a temperature between 200 °C and 400 °C, and exposed to air, it adsorbs oxygen on his surface. The adsorption process reduces the number of free electrons available in the metal oxide semiconductor and generates a depletion layer. When the oxygen adsorption process reaches an equilibrium, the resistivity of the sensing layer stabilises. The equilibrium state and, therefore, the sensor resistivity, depends on the type of metal semiconductor and on the heater temperature. This dynamic equilibrium is disturbed when the sensor is exposed to gases that can react with the oxygen. The gas molecules capture the oxygen molecules adsorbed onto the sensor surface, releasing electrons and changing the sensor resistivity.

For the Figaro sensors employed in this instrument, the relationship between the sensor electrical resistance, R_S, and the concentration of the sensed gas, C, under constant temperature and humidity, is given by the following empirical power-law relation:

$$R_S = A * C^{-\alpha} \quad (1)$$

where A is a constant specific to the oxide film, α is a constant specific to the film and the sensed gas. Rearranging equation 1, the concentration of a gas analysed by a MOS sensor can be estimated by measuring the sensor resistance, R_S. When the sample investigated is a complex mixture of gases, the sensor resistance is a result of the interaction of the sensor with all the different gases composing the sample.

For a given concentration of a vapour sample, the sensor resistivity depends on the temperature of the sensor heater element and on the humidity and temperature of the volatile sample. As a consequence, these parameters need to be carefully controlled to improve system sensitivity, reproducibility and discriminatory power.

To account for the humidity and temperature of the volatile sample, a humidity and temperature sensor, the Honeywell HIH-4602-C, was included in the system. The Honeywell sensor was enclosed in the custom measurement chamber together with the chemical sensors to detect the same temperature and humidity the MOS sensors are exposed to.

To control the temperature of the heater element, which fixes the temperature of the metal oxide semiconductor, a dedicated electronic sub-circuit has been designed. It is described and explained in section 3.2.2.

3.2. *Chemical sensor read-out circuit*

The electronic circuit of the test system is based on an inexpensive ATmega328P microcontroller and is composed of a few sub-circuits to power the sensor array, acquire the electrical resistance of the MOS sensors, control the MOS sensor heater elements, read the temperature and humidity sensor, and drive the sampling and delivery system. Sensor data are transferred by the microcontroller to a host PC for subsequent analysis.

Two sub-circuits, the sensor signal conditioning circuit and the sensor heater circuit are described below. The first one powers the sensors and acquires the sensor outputs. The second one controls and powers the sensor heater elements. These sub-circuits are key elements for optimising the sensitivity and the resolution of the instrument. Hence, instead of following the guideline suggested in the sensor datasheet for general sensor application, custom circuits were developed to enhance the capability of the instrument to detect small variations in the composition of the lubricant oil headspace.

3.2.1. Sensor signal conditioning circuit

A MOS sensor is a chemoresistive sensor that can be read by monitoring the change of its resistance, in response to the exposure to vapour samples. In this device, the interrogation happens by means of a potential divider.

The basic circuit of a voltage divider is shown in Figure 3, where R_S represents the variable sensor resistance, R_L is the load resistor and V_{DD} is the applied voltage.

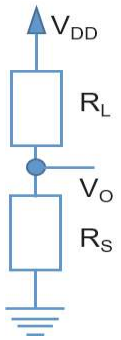

Figure 3. Basic voltage divider circuit. This circuit was modified and implemented in the artificial olfactory system to detect variations of the sensor resistance R_S.

This circuit reacts to changes in the sensor resistivity by changing the voltage divider output, V_O, according to equation (2):

$$V_O = R_S \frac{V_{DD}}{R_S + R_L} \quad (2)$$

Rearranging equation (2), the sensor resistance can be expressed as function of V_O:

$$R_s = R_L \frac{V_O}{V_{DD} - V_O} \quad (3)$$

and can be used to evaluate the concentration of the sensed gas, according to equation (1).

MOS sensor measurements are more often expressed by using the relative resistance ratio, R_r, instead of R_S. R_r, is defined in the equation (4):

$$R_r = \frac{R_S - R_o}{R_o} = \frac{\Delta R_S}{R_o} \quad (4)$$

where R_o, is the value of the sensor resistance at the beginning of the measurement, in reference air, before exposure to analyte, and R_s is the sensor resistance at the end of the measurement, when the sensor reaches the steady state after exposure to analyte. Normalising the sensor output as in equation (4) helps to compare sensors in the array that have considerably different base resistance values.

The voltage divider circuit implemented in this artificial olfactory device is more complex than the one in Figure 3. It is shown in Figure 4 and is composed of a Digital-to-Analog Converter (DAC) (U12) and two multiplexers (U3 and U11). The first multiplexer selects a load resistance choosing among six different resistors integrated in a thin film resistor network (labelled as R1 in Figure 4). The DAC provides the voltage to the divider circuit: its output is buffered and then applied to the load resistor selected by the multiplexer. The second multiplexer, U11, switches on the MOS sensor that needs to be acquired, connecting it in series to the selected load resistor. The voltage divider output is buffered with a second buffer (U2:B) and filtered before being connected to an Analog-to-Digital Converter (ADC), not shown in the picture, that digitizes the analogue voltage. The digitized voltage is fed into the microcontroller and the sensor resistance is calculated and saved.

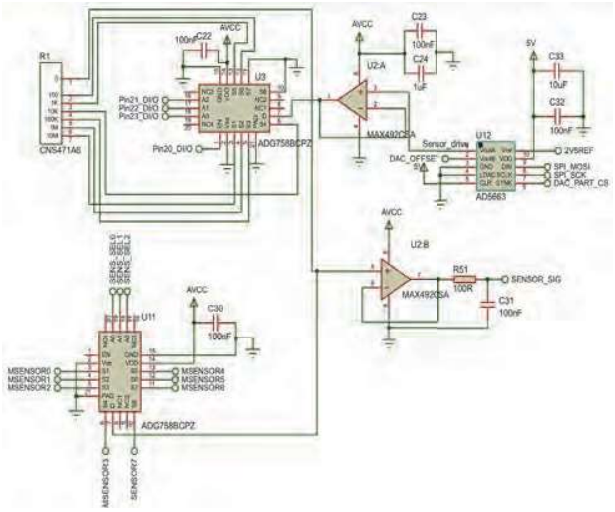

Figure 4. Voltage divider circuit designed to interrogate the MOS sensors.

The main difference between the circuits in Figure 4 and the one in Figure 3 is the replacement of the fixed load resistor R_L with the resistor network, R1. The network is composed of six resistors that span over six decades, from 100 Ω to 10 MΩ and allows to match the best load resistance for each sensor to improve the sensitivity and the resolution of the instrument.

The sensitivity of the voltage divider is defined as the ratio between the variation of the output voltage and the change in the sensor resistance. Using equation (2), the sensitivity of a voltage divider can be expressed as:

$$S = \frac{\partial V_o}{\partial R_S} = \frac{R_L}{(R_S + R_L)^2} * V_{DD} \quad (5)$$

A voltage divider that is characterised by high values of sensitivity will generate large variations of the output voltage, V_O, for small changes of the sensor resistance. Hence, maximising the sensitivity, S, of the voltage divider increases the resolution of the system and the overall capability of the electronic nose to detect small concentrations of the target gases.

Equation (5) shows clearly that the sensitivity depends on the load resistor. Calculating the first derivative of the sensitivity, S, with respect to R_L, for a fix value of R_S, and equating it to zero, it is found that the voltage divider sensitivity assumes the maximum value when the condition in equation (6) is verified:

$$R_S = R_L \quad (6)$$

Because R_S is not known a priori and its value changes during the measurement, it is inefficient to use a fixed value for the load resistor if the sensitivity of our system needs to be maximised.

The circuit shown in Figure 4 permits the selection of the load resistor during the measurement, choosing among the six resistors composing the network. Hence, it is always possible to use the value of the load resistor that is the closest to the dynamic value of sensor resistance, so that the voltage divider sensitivity is as close as possible to the optimal value.

Each resistor in the network has a finite value and can be the optimal one for a range of sensor resistances. Table 1 lists the load resistors and the ranges of the sensor resistances they match best. The limits of these ranges are used by the software to dynamically select the best load resistor for each sensor, during the experiments.

Load Resistor (R_L)		*Sensor resistance range matched*				
100	Ω			R_S	≤	316.23 Ω
1	kΩ	316.23 Ω	<	R_S	≤	3.16 kΩ
10	kΩ	3.16 kΩ	<	R_S	≤	31.62 kΩ
100	kΩ	31.62 kΩ	<	R_S	≤	316.23 kΩ
1	MΩ	316.23 kΩ	<	R_S	≤	3.16 MΩ
10	MΩ			R_S	>	3.16 MΩ

Table 1. The table shows which element of the voltage divider resistor network (first column) is chosen as load resistor for different ranges of the sensor resistance (second column). The choices highlighted in the table, provide the maximum value of the voltage divider sensitivity. For example, for R_S=15 kΩ, the load resistor that produces the maximum sensitivity is R_L=10kΩ**.**

Coupling the load resistor and the sensor resistor as highlighted in the Table 1, the error on the relative resistance reading, R_r, is limited to a maximum of 83.6 ppm. This is demonstrated in the following, by considering the resolution of the ADC used in the circuit and by introducing a parameter α as in equation (7):

$$R_L = \alpha R_S \tag{7}$$

The parameter α indicates the level of mismatch between R_L and R_S. If α=1, R_L=R_S; if α<1, R_L<R_S; if α>1, R_L>R_S. The higher the difference between α and 1, the higher the mismatch between R_L and R_S.

The ADC used for acquiring the analogue output of the voltage divider is a 24-bit sigma-delta ADC with 3 fully differential inputs or 5 pseudo differential inputs. Its corner frequency is set at 200 Hz. As reported on the component's datasheet, at this corner frequency the 24-nominal resolution is reduced to an effective number of 16-bits.

The number of the bits of the ADC limits the smallest voltage output change that the system can read, $\Delta V_{o(MIN)}$, according to equation (8):

$$\Delta V_{O(MIN)} = \frac{V_{DD}}{2^{Number\ of\ bits}-1} = \frac{V_{DD}}{2^{16}-1} = \frac{V_{DD}}{65535} \tag{8}$$

Using equation (5), $\Delta V_{O(MIN)}$ can be expressed by equation (9)

$$\Delta V_{O(MIN)} = S * \Delta R_{S(MIN)} = \frac{R_L}{(R_S+R_L)^2} * V_{DD} * \Delta R_{S(MIN)} \tag{9}$$

Rearranging equation (9) and using the equations (7) and (8), the minimum value of the relative sensor resistance that can be read by the system is:

$$\left(\frac{\Delta R_S}{R_S}\right)_{MIN} = \frac{(1+\alpha)^2}{\alpha * 65535} \tag{10}$$

$(\Delta R_S/R_S)_{MIN}$ versus α is plotted in Figure 5 to highlight how the mismatch between the load and the sensor resistance, quantified by α, determines the resolution of the artificial olfactory system.

The larger the difference between R_L and R_S, the larger the uncertainty on the relative resistance reading.

Figure 5 shows that for α = 1, the error on the relative sensor resistance is minimum, $(\Delta R_S/R_S)_{MIN}$ is equal to 61 ppm and the system resolution is the best one achievable reading the voltage divider output with the effective 16-bit ADC.

However, during an odour analysis, the sensor resistance can change in a range that is specified in the sensor datasheet. For these MOS sensors, the maximum range spans over two decades. This means that, in the worst case scenario, the difference between the load and sensor resistance is equal to 2 decades, or α=100, and $(\Delta R_S/R_S)_{MIN}$ =1556 ppm. Hence, in the worst case, the minimum detectable change in the sensor resistance is about 0.15% of its value.

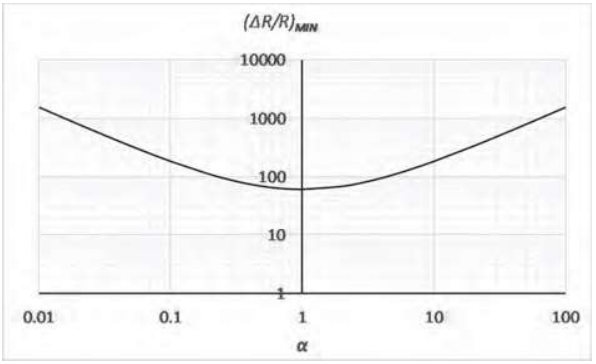

Figure 5. Plot of $(\Delta R_S/R_S)_{MIN}$ versus α, depicted on a log-log scale. The figure shows clearly that the minimum value of $(\Delta R_S/R_S)_{MIN}$ is achieved when α=1, which means that R_L = R_S.

If the load resistance is chosen at the beginning of the measurement and kept constant during the measurement, 1556 ppm is the resolution of sensor interface. However, if the load resistor is changed dynamically during the measurement, the resolution of the instrument can be improved. In fact, the voltage divider network, R1, has six elements and each element is one decade higher than the previous element. Hence, each sensor resistance can be coupled with a load resistor that differs from it of no more than half a decade, reducing the maximum value of α to 3.16. For this value of α, the resolution of the sensor interface corresponds to 83.6 ppm. This also corresponds to the theoretical minimum detectable resistance change in the worst case.

To achieve this value of resolution, a two-phase measurement process is implemented. During a first cycle of measurements, called "calibration", the system is exposed to clean air and the best load resistor is chosen, by software, for each sensor, among the six resistors in the network. After this phase, the measurement phase is started and the sensor is exposed to the vapour sample. The MOS sensor resistances change and they are acquired by the sensor interface. Their value is constantly compared with the range limits reported in the second column of Table 1. When a sensor resistance goes out of the initial range - selected during the calibration phase - the new best load resistor is chosen, according to Table 1.

It can be concluded that the designed read-out circuit and the process of dynamically selecting the best load resistor ensures that:

- the sensitivity of the voltage divider is always close to the best value;
- the resolution approaches the optimal value;
- the temperature and humidity of the volatile sample is monitored and any variation in the sensor response due to the variation of such parameters can be compensated during the data processing.

3.2.2. Sensor Heater circuit

It has been already demonstrated that the temperature of the metal oxide semiconductor, which is determined by the voltage applied to the heater element, influences the sensitivity and specificity of the sensor [41]. The datasheet of the MOS sensors suggests powering the heater element with 5V. However, this

might not be the value that optimises the sensitivity of the sensors to target analytes. Hence, we designed the heater circuit in Figure 6, which allows to apply a variable voltage to each sensor heater. The heater voltage can be selected in a range between 0V and the maximum value that is tolerable by the heating element.

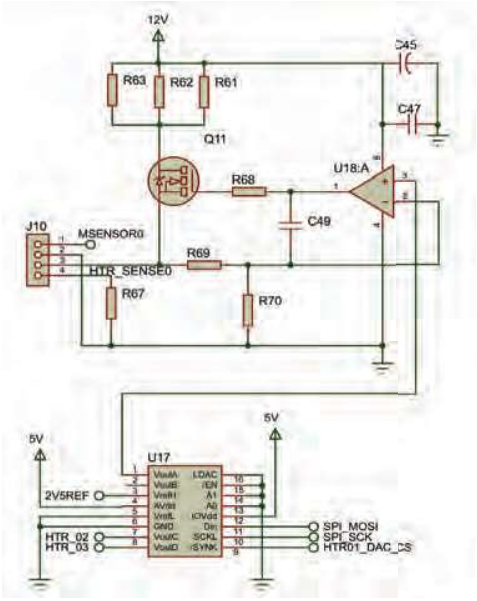

Figure 6. Custom-made sub-circuit designed to power the sensor heater elements

The main elements of the circuit are the op-amp U18:A, which drives the gate of a MOSFET (Q11), and the 2 resistors, R_{69} and R_{70}. The MOSFET provides the required current to the sensor heater. The U17 element is a DAC device, which is controlled by the main microcontroller and provides a reference voltage to the positive input of the op-amp. The op-amp negative input is wired to R_{69} and R_{70}. These resistors are connected in parallel to the heater element and determine the voltage applied to the heater.

Acting on the DAC output voltage, the voltage across the heater element of the MOS sensor is chosen and the metal oxide semiconductor temperature is selected.

3.3. *Measurement chamber*

The purpose of the measurement chamber is to hold the sensors in a sealed environment, where they can be exposed to the gas or vapours to be measured or to a reference gas to recover to their initial working point before starting a new measurement. The main objective in the design of the measurement chamber is to ensure a homogeneous flow over each sensor, avoiding the existence of regions where the flow is recirculating or stagnating. In addition, it is important that the chamber geometry does not induce a position dependent response.

This is particularly important for the MOX sensors, which internally operate at very high temperatures, in the range of 200 – 400 °C. This locally high temperature could interact with the gas flowing over the sensors and modify its physical and/or chemical characteristics. For this reason, it is desirable that the portion of gas flowing over a certain sensor does not reach any other sensor before leaving the measurement chamber.

A study of the motion of gas through the sensor chamber was performed using CFD analysis to solve the Navier-Stokes equation while considering the fluid to be incompressible, corresponding to:

$$\rho\frac{\partial u}{\partial t}-\eta\nabla^2\mathbf{u}+\rho(u\cdot\nabla)\mathbf{u}+\nabla p=\mathbf{F} \quad (11a)$$

$$\nabla\cdot\boldsymbol{u}=0 \quad (11b)$$

where ρ is the fluid density, **u** is the velocity field, η is the dynamic viscosity, p is the pressure and **F** is a volume force field (such as the gravity force field, ρ·g) neglected in this case. The equation (11a) is the momentum balance, while (11b) is the continuity equation for incompressible fluids. To completely describe the fluid-dynamic problem it was necessary to define a set of boundary conditions. The following conditions were used:

- A flow of 100 $cm^3 \cdot min^{-1}$ at the inlet of the measurement chamber, with a fully developed laminar (parabolic) profile;
- An outflow condition, implying that the total force on the output boundaries is a pressure force exerted by the ambient pressure and that the viscous force is zero;
- A "no slip" condition, applying to the internal walls and constraining the fluid velocity to be equal to the velocity of the walls. This implies that in the proximity of these boundaries, the fluid velocity drops to zero.

The simulated gas was air at standard ambient temperature and pressure (T=298.15 K, p=100 kPa).

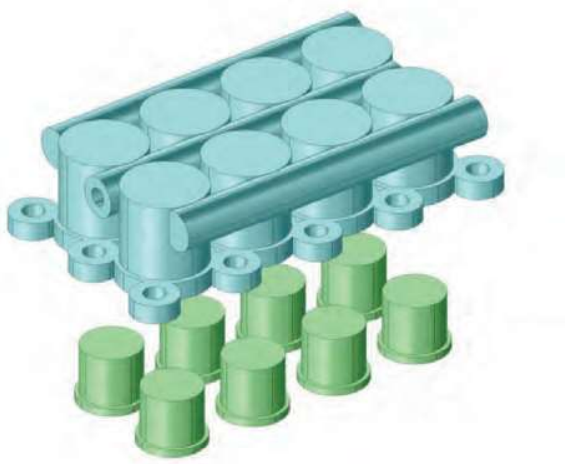

Figure 7. Proposed design of the measurement chamber, together with a sketch of the eight sensors in their TO5

Figure 7 depicts the proposed design of the measurement chamber. It is composed of a manifold to hold the eight sensors in the bottom part, with an o-ring (not shown in the drawing) surrounding each sensor to ensure the chamber was airtight.

The measurement chamber was screwed to a PCB, to keep the sensors and the o-rings compressed against the manifold and route the connections to the sensors.

The measurement chamber was designed so that the gas enters through a central channel, and then splits from there in eight distinct flows. Each flow passes over one sensor only and exits the sensor chamber through one of the two lateral channels.

Figure 8 shows the internal volume of the gas flow, together with the mesh generated for the CFD analysis. The total volume of this region is 2.25 cm^3.

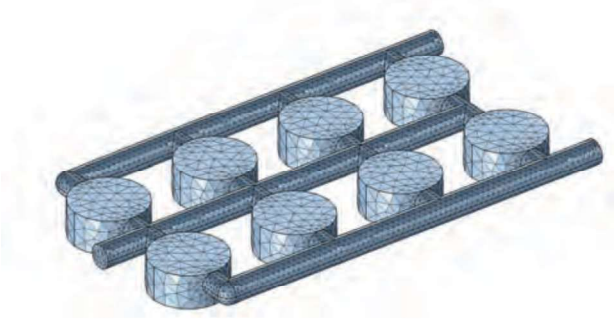

Figure 8. The picture shows the internal volume of the sensor chamber where the gas can flow, together with the mesh generated to solve the fluid-dynamic simulation.

Figure 9 illustrates the results of the CFD analysis showing the streamlines of the flow velocity field. The colour of the streamlines corresponds to the speed of the gas. It is possible to see how the gas flows through the central channel reducing its speed gradually, while entering each sensor space at a much reduced and almost constant speed. Once the streamlines exit a sensor seat, they enter one of the two lateral channels, never flowing across another sensor, confirming the absence of cross-contamination. Finally, it is possible to confirm that the flow is laminar all over the internal volume of the measurement chamber and there are neither recirculation regions nor stagnation zones.

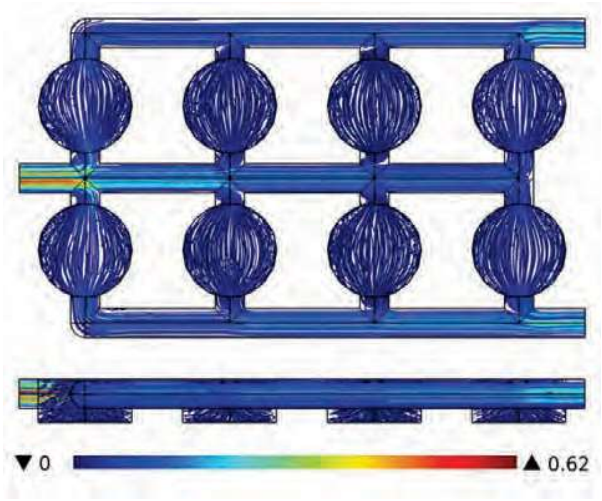

Figure 9. Streamlines of the velocity field. The colour of the streamlines represents the speed of the fluid, in m/s.

4. Data collection

Initial laboratory measurements were carried out on the system to test its ability to:

- produce repeatable measurements;
- provide sensor patterns that are characteristics of the sample under test.
- discriminate between new and aged oil.

The tests were performed on water samples, aged engine oil and new engine oil samples.

For these experiments, the sampling system shown in Figure 10 was built. It comprises a flow meter, two 3-way valves and a gas pump, and allows a measurement cycle composed of two phases: cleaning and measurement. The valves select two different paths, depending on the measurement phase. During the cleaning phase, ambient air is delivered directly to the sensors (through the upper path of the system in Figure 10) without passing through the sample vial. This phase is used to build a stable sensor baseline before starting the measurement: the equilibrium between the oxygen molecules adsorbed on the sensing layer and those desorbed from the layer can be established. When a stable baseline is obtained, the measurement phase starts. The valves select the alternative path (the lower path of the system in Figure 10). The ambient air passes through the glass vial, which contains the liquid analyte sample, and carriers to the sensors the volatile compounds emitted by the liquid sample.

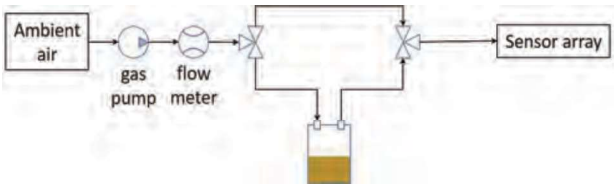

Figure 10. The picture shows the sampling system designed and built for the initial measurements.

The gas pump fixes the air flow to 200 sccm. Variations in the sample flow rate would affect the sensor response. Hence, a flow meter was included in the delivery system to monitor and control the flow.

The delivery system and the custom measurement chamber ensure homogeneous flow over each sensor; avoid analyte contamination and recirculation or stagnation of the flow and guarantee that the portion of the gaseous sample flowing over a certain sensor does not reach any other sensor before leaving the chamber.

During the measurements, the sensor signals were sampled every 1 sec and are saved on an external PC. Unfortunately, in these tests one of the MOS sensor in the array was found not to work. Hence, only six chemical sensors were used for these initial tests.

Three different analytes were used for the tests:

- Water sample, used as reference;
- New SAE 10W - 40 engine oil;
- Used SAE 10W - 40 engine oil from a Formula Ford racing which had run for 450 miles.

Three glass vials were prepared for the experiments, by filling each of them with 10 ml of one of the analyte. All the vials were kept at room temperature during the measurements.

For each analyte, repeated and not sequential measurements were carried out. Table 2 list the number of measurements for each sample.

Sample	***Number of Repetitions***
Water	8
New Oil	9
Used Oil	7

Table 2. The table summaries the number of repetitions carried out for each sample.

The sensor pattern generated by each measurement was saved on a host PC and processed as described in the following section.

5. Analysis of the results and discussion

The first characteristic that was assessed was the sensor repeatability, which is essential for any measurement or analytical instrument. Higher levels of repeatability allow a higher discrimination capability for a device.

The evaluation was made by examining the response of the sensing elements over the replicated trials. For each measurement, the relative resistance expressed as in equation 4 was calculated.

Figure 11 to Figure 13 depict the response of one sensor of the array, labelled as S2, to two repetitions of new oil, aged oil and water, respectively.

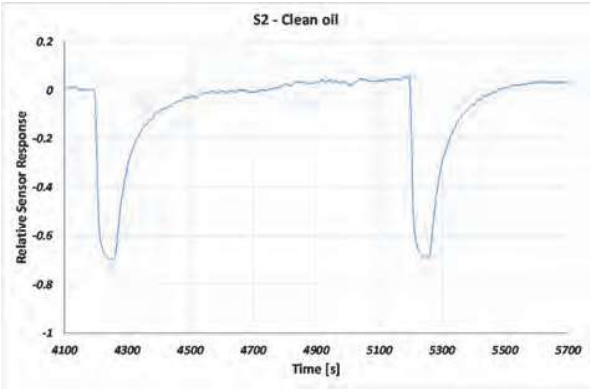

Figure 11. The figure shows the response generated by the second sensor in the array, S2, when exposed to clean oil sample.

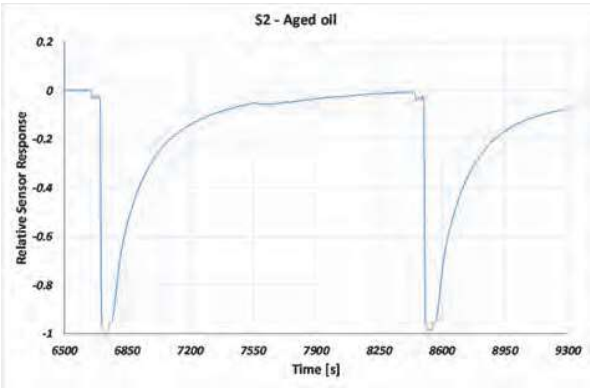

Figure 12. The figure shows the response generated by the second sensor in the array, S2, when exposed to aged oil sample.

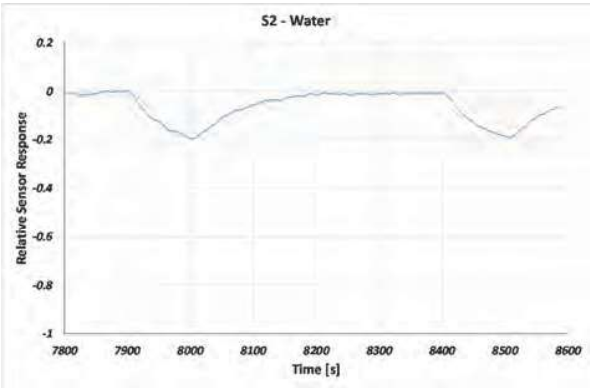

Figure 13. The figure shows the response generated by the second sensor in the array, S2, when exposed to a water sample.

The figures show that the sensor responses generated by the artificial olfactory system appear similar among the replicates, indicating a good level of repeatability.

The figures also show that the same sensor reacts in a different way when it is exposed to the different analytes, generating a sensor signal that is characteristic of the volatile compounds of the sample's headspace. This is true for all the sensors of the array.

Figure 14 shows the sensor patterns generated by the three different samples. The feature used to build the bar plots were obtained by calculating the logarithm of the ratio between the sensor resistance at the end of the measurement when a steady sensor signal was generated and the sensor resistance before starting the measurement at the stable baseline. This feature was used because it allowed comparison and represented, on the same plot, the response of sensors exhibiting very different resistance values to those in our device.

Inspecting the graphs in Figure 14, it can be stated that:

- The sensor patterns of the two sample oils have an intensity which is much higher than the one associated to the reference sample. This behavior confirms that the sensors have high sensitivity to the lubricant volatile compounds.
- The sensor pattern generated by the used oil is significantly different to the one generated by the new oil. Hence, this artificial olfactory instrument seems to be capable of detecting the variation in the volatile compounds of the lubricant headspace due to the degradation process.
- One of the sensors in the array has a decreased intensity of the feature considered, while the other sensors show an increased intensity. During degradation, the relative concentration of the volatile compounds in the lubricant headspace changes. As explained above, the sensor response depends on the whole composition of the sample. Hence, depending on the change of the relative concentration of competitive gases, the sensor response to aged oil can be higher than that generated by the new oil or can be lower. It is the entire composition of the sample that determines the sensor signal, and this is a crucial ability of the system to detect differences in the complex oil matrix.

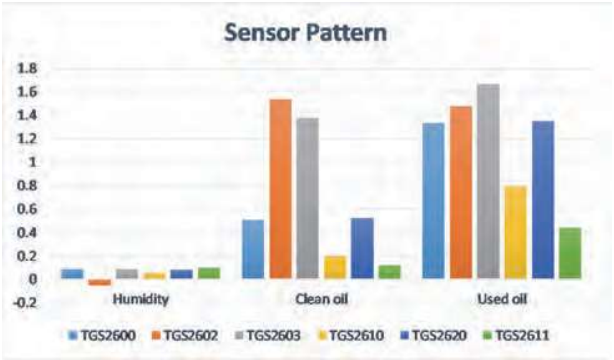

Figure 14. The picture shows the sensor patterns generated by the array when analyzing the three different samples, water, on the left, new oil, in the center, and used oil on the right.

The last analysis carried out was aimed at verifying that the artificial olfactory system could discriminate between old and new oil. Principal component analysis (PCA) was used to process the feature introduced for the bar plot. PCA is an unsupervised or explorative method that 'explore' the sensor responses, trying to determine if there is any 'natural' classification significant for the

case of interest. It is a statistical procedure that reduces the data dimensionality and transforms the original coordinate system of correlated variables (the sensor space) into a new system of uncorrelated variables, called principal components (PC). This allows the representation of the sensor data in a system of reduced dimensionality. The plot produced is called "score plot". Normally, the first two or three PCs are enough to represent the information and it is possible, in this reduced space, to evaluate, by means of visual inspection, if an intrinsic clustering of the data exists [42].

In Figure 15 the score plot generated by processing the sensor data with the PCA, is shown.

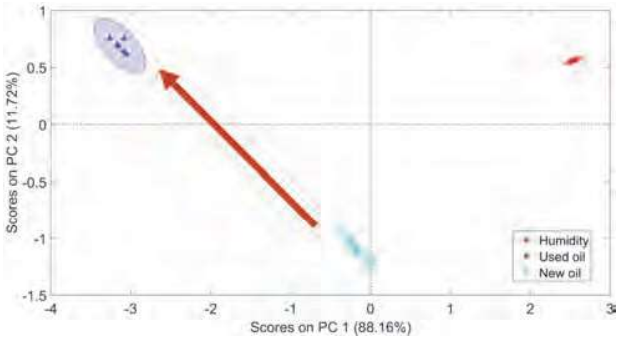

Figure 15. The score plot was created by applying PCA to sensor patterns generated during the measurements. Three clusters are visible on the score plot. Each cluster, which is composed of measurements carried out on the same sample, is completely separated from the other clusters. Hence, the PCA confirmed that the e-nose generated 'fingerprints' of the three different odours tested.

The plot shows that, not only is the water sample completely discriminated from the oil sample, but also that the cluster of the aged oil is completely separated from the new oil cluster.

Hence, these tests seem to demonstrate that the artificial olfactory system can monitor the oil aging process and that the optimization process used in design improves its discriminatory power. The process also seems to be sensitive, considering that the aged oil is engine oil that was used for a short run, only 450 miles.

More experiments are needed to be able to perform a complete characterization of the artificial olfactory system and be able to provide details on resolution and sensitivity towards the oil degradation process. However, these initial results are highly promising.

6. Conclusion

In this paper, the development of an artificial olfactory system for oil health monitoring by headspace analysis has been described.

Artificial olfactory systems present several advantages over the traditional analytical methods: they are cheap and easy to use, can be used in harsh environments, have small dimensions and they can carry out rapid, real-time analysis. Hence, this technology can potentially overcome some of the disadvantages of the alternative strategies commonly used for oil degradation analysis.

The core of e-nose instruments is the array of chemical sensors. Among the large variety of sensor technologies available nowadays, we choose for this system metal oxide sensors which are stable, robust and have high sensitivity towards the analytes that are characteristic of the degradation process.

To improve the capability of the instrument in carrying out oil condition monitoring, a custom-made electronic circuit and measurement chamber were designed.

The electronic circuit allowed the sensors to work under optimal conditions: maximum sensitivity, low value of resolution, and rapid measurements execution. The strategies adopted to achieve these goals have been detailed and demonstrated in the paper.

The measurement chamber has been designed with the aid of CFD simulations. The simulation results have been discussed in the paper and demonstrate that the geometry of the chamber assures that the main flow entering the chamber is split in eight distinct flows. Each flow is laminar and passes only over one sensor at a reduced and almost constant speed. Hence, there is no cross contamination among the sensors, stagnation zones or recirculation. Variations in the sensor response are due only to the analyte composition.

The system has gone through initial laboratory testing. A simple sampling system was developed to deliver the headspace gas from the sample under test to the sensor array. Ambient air was used as carrier gas and the samples were kept in a vial at room temperature.

The results of these measurements are highly promisingly and can be summarised:

- The measurements were highly reproducible. Very similar sensor patterns were generated when the same sample was analysed
- different sensor patterns were produced when different analytes were measured;
- PCA analysis showed that measurements of the same sample types form a cluster which is completely separated from the clusters generated by different types of samples;
- Very good discrimination between new and aged oil was achieved. The aged oil was used in a car engine that ran only for 450 miles, but it generated sensors responses very different from those produced by new oil. This suggests the system can differentiate degradation stages that are very close to each other.

These measurements are only initial tests. They show that, thanks to the optimization strategies adopted, this artificial olfactory instrument has great potential for real-time oil degradation monitoring.

Several new and different measurements have been planned to have a complete characterization of the system capabilities.

Laboratory tests will be carried out on several oil formulations at different stages of degradation. These measurements, besides giving a clearer understanding of the capability of the system to discriminate between close degradation stages of the oil, will permit the building of a large dataset for advanced data analysis. The system will be also tested in lab in conjunction with a friction test machine and in operating machine elements such as a gearbox.

For these experiments, sampling systems will be developed to make the system suitable for use under real-life conditions

References

1. Sharma B.C. and Gandhi O.P., (2008), Performance evaluation and analysis of lubricating oil using parameter profile approach, Industrial Lubrication and Tribology, Vol. 60, Issue 3, 131 - 137.

2. Du Y., Wu T., Cheng J, (2015), Age Detection of Lubricating Oil with On-line Sensors, in Proc. 2015 IEEE SENSORS, Busan, Korea.
3. Zhu X., Du L., Liu B., Zhe J. (2016), A microsensor array for quantification of lubricant contaminants using a back propagation artificial neural network, Journal of Micromechanics and Microengineering, Vol. 26, Issue 6.
4. Zhu X., Zhong C., and Zhe J., (2017), Lubricating oil conditioning sensors for online machine health monitoring – A review, Tribology International, Vol. 109, 473–484.
5. Levermore D.M., Josowicz M, Rees W.S., and Janata J., (2001), Headspace analysis of engine oil by gas chromatography/mass spectrometry, Anal Chem Vol. 73, Issue 6, 1361–1365.
6. Rök, F., Barsan, N., Weimar, U., (2008), Electronic nose: current status and future trends, Chem. Rev., Vol. 108, Issue 2, 705-725.
7. Pearce T. C., Schiffman S. S., Nagle H. T., and Gardner J. W., (2003), Handbook of Machine Olfaction - Electronic Nose Technology, edited by John Wiley & Sons.
8. Zhu J., He D., Bechhoefer E., (2013), Survey of lubrication oil condition monitoring, diagnostics, prognostics techniques and systems, Journal of Chemical Science and Technology, Vol. 2 Issue 3, 100-115.
9. Soleimani, M., Sophocleous, M., Wanga, L., Atkinson, J., Hosier, I.L., Vaughan, A. S., Taylor, R.I., Wood R.J.K., (2014), Base oil oxidation detection using novel chemical sensors and impedance spectroscopy measurements, Sensors and Actuators B, Vol. 199, 247–258.
10. Soleimani M., (2014) Thick Film Sensors For Engine Oil Acidity Detection, . PhD Thesis, University of Southampton,UK.
11. Soleimani, M., Sophocleous, M., Glanc, M., Atkinson, J., Wanga, L., Wood R.J.K., Taylor, R.I., (2013), Engine Oil Acidity Detection Using Solid State Ion Selective Electrodes, Tribology International, Vol.65, 48-56.
12. Zhu X., Du L., Zhe J., (2014), An integrated lubricant oil conditioning sensor using signal multiplexing, J. Micromech. Microeng. Vol. 25, Issue 1.
13. Du, L. and Zhe J., (2012), Parallel sensing of metallic wear debris in lubricants using undersampling data processing, Tribology International, Vol. 53, 28-34.
14. Bley, T., Pignanelli, B., Schütze, A., (2014), Multi-channel IR sensor system for determination of oil degradation, Journal of Sensors and Sensor Systems, 3, 121–132.
15. Deshmukh S., Bandyopadhyay R., Bhattacharyya N., Pandey R.A, Jana A., (2015), Application of electronic nose for industrial odors and gaseous emissions measurement and monitoring – An overview, Talanta, Vol.144, 329-340.
16. Bernabei M., Pantalei S., Persaud K.C., (2016) Large-Scale sensor array for machine olfaction, Chapter 3 in Essentials of Machine Olfaction and Taste, Nakamoto T., John Wiley & Sons Singapore Pte Ltd.
17. Bernabei M., Beccherelli, R., Zampetti E., Pantalei S., Persaud K.C., (2013) Mimicking Biological Olfaction with Very Large Chemical Arrays, Chapter 3 in Neuromorphic Olfaction, Persaud, K.C., Marco S., Gutierrez-Galvez A., Taylor and Francis Group, London.
18. Wilson, A.D. (2014), Identification of insecticide residues with a conducting-polymer electronic nose, Chem. Sens., Vol. 4, Issue 3, 1–10.
19. Son M., Cho D., Lim J. H., Park J., Hong S., Ko H. J., Park T.H, (2015), Real-time monitoring of geosmin and 2-methylisoborneol, representative odor compounds in water pollution using bioelectronic nose with human-like performance, Biosensors and Bioelectronics, Vol 74, 199-206.
20. Abbas M.N.; Moustafa G.A.; Gopel T.V., (2001) Multicomponent analysis of some environmentally important gases using semiconductor tin oxide sensors. Anal. Chim. Acta, Vol. 431, 181–194.
21. Baby R.E., Cabezas M., Walsöe de Reca E.N., (2000) Electronic nose: a useful tool for monitoring environmental contamination, Sensors and Actuators B: Chemical, Vol 69, Issue 3, 214-218.
22. Cali K., Bernabei M., Persaud K., (2015) Development of mutant Odorant Binding Proteins (OBPs) for Security Applications: Detection of Explosives and Drugs. in CHEMICAL SENSES. vol. 40, 266-267.
23. Brudzewski K., Osowski S., Pawlowski W., (2012), Metal oxide sensor arrays for detection of explosives at sub-parts-per million concentration levels by the differential electronic nose, Sensors and Actuators B: Chemical, Vol. 161, Issue 1, 528-533.
24. Dymerski, T., Gebicki, J., Wardencki, W. and Namiesnik, J. (2013). Quality evaluation of agricultural distillates using an electronic nose. Sensors (Basel). Vol. 13, 15954–15967.
25. Wilson, A.D., Diverse applications of electronic nose technologies in agriculture and forestry, (2013) Sensors, Vol.13, Issue 2, 2295-2348.
26. Baldwin, E.A.; Bai, J.; Plotto, A.; Dea, S., (2011), Electronic noses and tongues: Application for the food and pharmaceutical industries, Sensors, Vol.11, Issue 5, 4744–4766.
27. Ryan, M.A.; Manatt, K.S.; Gluck, S.E.; Shevade, A.V.; Kisor, A.K.; Zhou, H.; Lara, L.M.; Homer, M.L., (2009) Operation of Third Generation JPL Electronic Nose on the International Space Station; SAE Technical Paper 2009-01-2522; Jet Propulsion Laboratory, California Institute of Technology: Pasadena, USA.
28. Ryan M.A., Zhou H., Buehler M.G., Manatt K.S., Mowrey V.S., Jackson S.P., Kisor A.K., Shevade A.V., Homer M.L., (2004), Monitoring Space Shuttle Air Quality Using the JPL Electronic Nose, IEEE Sensors Journal, Vol. 4, Issue 3, 337-347.
29. Santonico M., Pittia P., Pennazza G., Martinelli E., Bernabei M., Paolesse R., D'Amico A., Compagnone D., Di Natale C., (2008) Study of the aroma of artificially flavoured custards by chemical sensor array fingerprinting, Sensors and Actuators B: Chemical, Vol. 133, Issue 1, 345-351.
30. Chatterjee, D., Bhattacharjee, P., Bhattacharyya, N., (2014), Development of methodology for assessment of shelf-life of fried potato wedges using electronic noses: sensor screening by fuzzy logic analysis, Journal of Food Engineering, 133, 23–29.
31. Güney, S. and Atasoy, A. (2015). Study of fish species discrimination via electronic nose. Comput. Electron Agric., Vol. 119, 83–91.
32. Lim J.H., Park J., Ahn J.H., Jin H.J., Hong S., Park T.H., (2013) A peptide receptor-based bioelectronic nose for the real-time determination of seafood quality, Biosens. Bioelectron., Vol 39 244–249.
33. Labreche S., Bazzo S., Cade S., Chanie E, (2005) Shelf life determination by electronic nose: application to milk, Sensors and Actuators B: Chemical, Vol. 106, Issue 1, 199-206.
34. Tsai E., (2004), Flavor analysis in a pharmaceutical oral solution formulation using an electronic-nose, Journal of Pharmaceutical and Biomedical Analysis, Vol 34, 453–461.
35. Guo D., Zhang D., Li N., Zhang L., and Yang J., (2010) A Novel Breath Analysis System Based on Electronic Olfaction, IEEE Transactions on Biomedical Engineering, vol. 57, Issue. 11, 2753-2763.
36. D'Amico A., Di Natale C., Paolesse R., Macagnano A., Martinelli E., Pennazza G., Santonico M., Bernabei M., Roscioni C., Galluccio G., Bono R., Finazzi Agrò E., Rullo S., (2008), Olfactory systems for medical applications, Sensors and Actuators B: Chemical, Volume 130, Issue 1, .458-465.
37. Bernabei M., Pennazza G., Santonico M., Corsi C. Roscioni C., Paolesse R., Di Natale C., D'Amico A.. (2008) A preliminary study on the possibility to diagnose urinary tract cancers by an electronic nose, Sensors and Actuators B: Chemical, Vol. 131, Issue 1, 1-4.
38. Herman-Saffar O, Boger Z., Libson S., Lieberman D., Gonen R., Zeiri Y.,(2018) Early non-invasive detection of breast cancer using exhaled breath and urine analysis, Computers in Biology and Medicine,Vol. 96, 227-232.
39. Greulich T., Fischer H., Lubbe D., Nell C., Ingo Baumbach J., Koehler U., Boeselt T., Vogelmeier C., Koczulla A.R., (2018), Obstructive sleep apnea patients can be identified by ion mobility spectrometry-derived smell prints of different biological materials, Journal of Breath Research, Volume 12, Issue 2.
40. Chan D.K., Leggett C.L, and Wang K.K, (2016), Diagnosing gastrointestinal illnesses using fecal headspace volatile organic compounds, World J Gastroenterol., Vol. 22, Issue 4, 1639–1649.
41. Fort, A., Gregorkiewitz, M., Machetti, N., Rocchi, S., Serrano, B., Tondi, L., Ulivieri, N., Vignoli, V., Faglia, G., Comini, E., (2002), Selectivity enhancement of SnO2 sensors by means of operating temperature modulation, Thin Solid Films, Vol. 418, Issue 1, 2-8.
42. Hines E. L., Boilot P., Gardner J.W., Congora M.A.,(2003) Pattern Analysis for Electronic noses in Handbook of Machine Olfaction – Electronic Nose Technology, T.C. Pearce, S. S. Schiffman, H.T. Nagle, J.W.Gardner, Eds. 2003, 133-160.